A Topologically Inspired Path-Following Method With Intermittent State Feedback

Sage C. Edwards, Duc M. Le, Dan P. Guralnik, and Warren E. Dixon

***Abstract*—Autonomous systems often operate in environments where state feedback may not be available, such as in anti-access and area denial environments. In these environments, it is often required that an agent track a path, despite interruptions in state feedback. As a result, the class of *Relay-Explorer* problems has emerged, where a switched system approach is used to account for intermittent state feedback. Past work on these problems established a framework for developing dwell-time conditions for stable tracking using these methods. However, existing work only applies to a limited class of reference paths and feedback region geometries. This letter advances a topologically inspired method for guaranteeing re-acquisition of feedback for nearly arbitrary geometries in arbitrary dimensions, all while relaxing the dwell-time conditions and retaining the uniformly ultimately bounded stability result from preceding work. Numerical experiments in the plane demonstrate an increase of hundreds of percentage points—even for fairly generic geometries—in the tracking error the agent could afford, using the proposed method, without sacrificing stability.**

***Index Terms*—Computational geometry, hybrid logical/dynamical planning and verification, motion and path planning.**

I. Introduction

STATE feedback is a critical component in designing path-planning methods used for guidance, navigation, and control of autonomous vehicles. Factors such as task definition, operating environment, sensor modality, and adversarial effects may result in intermittent state feedback, inhibiting a system's ability to achieve its task. For mobile platforms, one prominent approach to overcoming difficulties with obtaining state feedback is to design controllers and planners that enable computation of the state from available observations (see [1] in the context of visual servoing, and [2] in a SLAM setting). Other approaches arise in network control, where limitations on communication and communication delays affect the stability of the system (see [3] in the context of time-varying connectivity and [4] for an event triggered approach).

An emerging body of work embraces these difficulties by considering them as a class of *Relay-Explorer* problems. Using a switched system approach, control laws are constructed which use state feedback for navigation when available (stabilizable mode), and open-loop state estimates otherwise (unstable mode). For example, in a single agent setting [5], to ensure stability, the agent has to repeatedly reacquire feedback by entering a fixed region where feedback is available. A time-varying feedback region may naturally arise in multi-agent settings. For example in [6], some agents may have the capability of relaying feedback information to feedback-denied members of their team by moving into communication radius.

Similar to the framework in [5], this letter considers a single agent tasked with tracking a desired path that may lie outside a known feedback region. State feedback is available when the agent is inside this region, and unavailable otherwise. Since the desired path may lie outside of the feedback region, the agent dead-reckons when feedback is not available. To achieve the task, a path-planning algorithm is designed to generate an auxiliary trajectory for the agent to track. The instabilities inherent to dead-reckoning impede the agent's ability to return to the feedback region. This forces the auxiliary trajectory to alternate between following the desired path and returning to the feedback region. This framework relies on a Lyapunov-based switched system analysis [7] to derive dwell-time conditions dictating the duration a system can remain in each operating mode while ensuring stability.

The predominant factor affecting dwell-time conditions in this setting is the need to guarantee re-acquisition of state feedback. To furnish this guarantee, results in [5] and [8] require the agent to dead-reckon to a point where the region of state uncertainty is contained within the feedback region—the *Inscribed Ball Criterion* (IBC). Crucially, these results only consider circular feedback regions where the dwell-time conditions only depend on the distance of the agent to the feedback region. However, applying the same approach to more general geometries—the expected norm in real-life applications—results in unnecessarily conservative bounds. For example, when an agent moves towards a long and narrow rectangular feedback region, Fig. 1 shows that a better strategy is to aim at a point beyond the region, affording a larger error margin at the target point. Intuitively, small perturbations in the shape of this region should not result in a change of strategy, motivating a topological approach. Moreover, it is clear that the preceding considerations could not be easily replicated for an arbitrary geometry of the feedback region, because of complex interactions between local properties (e.g., curvature at nearby boundary points) and global properties (e.g., concavities, spirals, etc.).

This letter addresses the need for generating re-entry guarantees for arbitrary geometries of the feedback region. To this end,

Manuscript received August 21, 2020; accepted February 20, 2021. Date of publication March 22, 2021; date of current version April 12, 2021. This letter was recommended for publication by Associate Editor N. Amato and Editor F. van der Stappen upon evaluation of the reviewers' comments. This work is supported in part by AFOSR Award Numbers FA9550-19-1-0169, FA9550-18-1-0109, NEEC Award Number N00174-18-1-0003, and in part by Office of Naval Research Grant N00014-13-1-0151. *(Corresponding author: Sage Edwards.)*

The authors are with the Department of Mechanical and Aerospace Engineering, University of Florida Gainesville, Gainesville, Florida 32611 USA (e-mail: sageedwards@ufl.edu; ledan50@ufl.edu; danguralnik@ufl.edu; wdixon@ufl.edu).

Digital Object Identifier 10.1109/LRA.2021.3067295

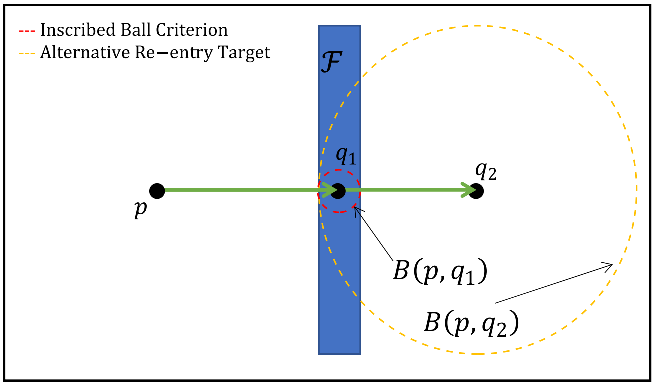

Fig. 1. Given a feedback region $\mathcal{F}$, an initial starting point p, and a target point $q_1 \in \mathcal{F}$, the ball $B(p, q_1)$ about q_1 inscribed in $\mathcal{F}$ represents the maximum allowed region of uncertainty based on IBC. For this geometry, a much larger region of uncertainty may be allowed for an overwhelming majority of starting points p, provided one does not insist on q_1 to lie in $\mathcal{F}$, replacing q_1 with q_2, for example.

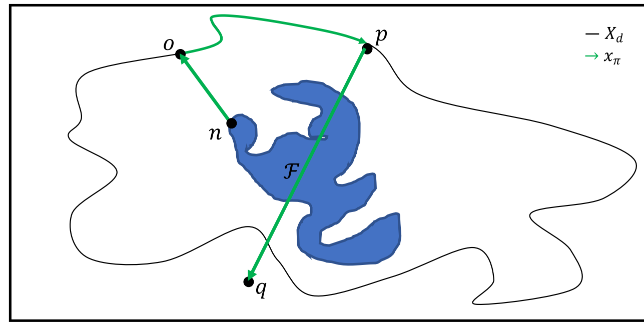

Fig. 2. The auxiliary trajectory x_π, defined by a path plan $\pi = (\mathrm{n, o, p, q})$, is superimposed over the desired path X_d, for a generic feedback region $\mathcal{F}$ (see Definition 1). Note that the point q need not lie in $\mathcal{F}$.

separation properties of embedded spheres in $\mathbb{R}^D$, $D \geq 2$ are deployed (Sections IV-A–IV-B). The resulting *Topological Re-entry Criterion* is applied to increase the maximum dwell-time by raising the upper bound on the allowed error growth, in a state-dependent fashion, while being cognizant of the geometry of the feedback region in the agent's vicinity (Sections IV-C–IV-E). The proposed framework generalizes the results in [5] from circular geometries in $\mathbb{R}^2$ to nearly arbitrary contractible geometries in $\mathbb{R}^D$ of the feedback region, by casting the problem of constructing auxiliary trajectories as an optimization problem (Section IV-D): selecting an optimal auxiliary trajectory is tantamount to computing, at every point of the desired path, the largest tracking error the agent can afford without losing the guarantee of return (the agent's *uncertainty budget* at that point). In particular, this framework guarantees uniformly ultimately bounded errors for repeated optimal choices of the auxiliary trajectories (Theorem 4). To assess the degree of improvement offered by the topological re-entry criterion over IBC an algorithm for computing uncertainty budgets is given in Section V and numerical studies in Section VI.

II. Problem Statement

A. Notation

For any integer $D \geq 1$, the Euclidean distance between $p, q \in \mathbb{R}^D$ is denoted by $\mathtt{dist}(p, q) \triangleq \|p - q\|_2$. Let $\mathbb{S}^{D-1}$ and $\mathbb{B}^D$ denote the Euclidean unit sphere and closed unit ball in $\mathbb{R}^D$, respectively. Given $p \in \mathbb{R}^D$ and $r > 0$, the open ball $B_r(p)$ of radius r about p is the set of $q \in \mathbb{R}^D$ with $\mathtt{dist}(p, q) < r$. The shortest distance from a point to a set is $\mathtt{dist}(p, A) \triangleq \inf\{\mathtt{dist}(p, q) : q \in A\}$. The diameter of $A \subset \mathbb{R}^D$ is $\mathtt{diam}(A) \triangleq \sup\{\mathtt{dist}(p, q) : p, q \in A\}$. The closure of $A \subseteq \mathbb{R}^D$ is denoted by $\mathtt{cl}(A)$. A point is an interior point of a set if $B_r(p) \subseteq A$ for some $r > 0$. The set of interior points of $A \subseteq \mathbb{R}^D$ is denoted by A°. A different notion of interior is associated with embeddings of $\mathbb{S}^{D-1}$ in $\mathbb{R}^D$, see (11).

B. Agent Dynamics

This letter considers an agent with dynamics modeled by

$$\dot{x} = f(x, t) + \zeta(t) + d(t), \tag{1}$$

where $x : \mathbb{R}_{\geq 0} \to \mathbb{R}^D$, $D \geq 2$, denotes the state; $f : \mathbb{R}^{\mathbb{D}} \times \mathbb{R}_{\geq 0} \to \mathbb{R}^D$ denotes locally Lipschitz drift dynamics; $d : \mathbb{R}_{\geq 0} \to \mathbb{R}^D$ denotes an exogenous disturbance; and $\zeta : \mathbb{R}_{\geq 0} \to \mathbb{R}^{\bar{D}}$ denotes a control input. The following assumption is used in the subsequent development.

Assumption 1: The exogenous disturbance d satisfies $\|d(t)\| \leq \bar{d}$ for all $t \in \mathbb{R}_{\geq 0}$, where $\bar{d} \in \mathbb{R}_{>0}$ is known. ■

C. Control Objective

Let $\mathcal{F} \subset \mathbb{R}^D$ denote a known region where state feedback is available, i.e., state feedback is available to the agent if and only if $x \in \mathcal{F}$. The *feedback region*$\mathcal{F}$ is modeled as the closure of the interior region of a polyhedral sphere C. Equivalently, $\mathcal{F}$ is the image of an embedding of $\mathbb{B}^D$ in $\mathbb{R}^D$ (see Section IV). The *feedback-denied region*, $\mathcal{F}^c \triangleq \mathbb{R}^D \setminus \mathcal{F}$, is the set of states where feedback is not available.

The agent is tasked with following a desired polygonal path X_d, which is provided as a sequence of way points $(\mathcal{P}_0, \ldots, \mathcal{P}_M)$ in $\mathbb{R}^D$, some of which may lie outside of $\mathcal{F}$. Repeated dead-reckoning along the sequence of way points is inherently unstable outside of $\mathcal{F}$. This motivates an approach where the agent follows a sequence of *auxiliary trajectories*, relaying between the desired path and the feedback region (see Fig. 2), to ensure the error system remains bounded.

Definition 1 (Auxiliary Trajectory): There are two types of auxiliary trajectories. The auxiliary trajectory $x_\pi : \mathbb{R}_{\geq 0} \to \mathbb{R}^D$ with path plan $\pi = (n, o, p, q)$, is defined as the concatenation of three trajectories determined by four way points: n is the point of departure from the feedback region; o is the first point along a segment of X_d the agent selects to follow; p is the point of departure from X_d; and q is the target point for the return trajectory to the feedback region. From n to o, and from p to q, x_π restricts to straight line trajectories[1] with constant speed v_0. From o to p, x_π coincides with the desired path X_d, with a piecewise linear parametrization of constant speed v_0. For the second type of auxiliary trajectory—with plan $\pi = (p, q)$—set

[1]Curved trajectories may improve performance, but outside our scope.

x_π to coincide with a linearly parametrized line segment from p to q with constant speed v_0.

Remark 1: Plans $\pi = (p, q)$ are used for acquisition of feedback from points $p \notin \mathcal{F}$, while plans $\pi = (n, o, p, q)$ are used for tracking X_d and reacquiring feedback. A plan terminates the moment feedback is reacquired.

Assumption 2: It is assumed that feedback acquisition is instantaneous upon re-entry into the feedback region. ■

Remark 2: Between the executions of two plans, the agent travels through $\mathcal{F}$, taking advantage of the available feedback. Two cases may occur. If the next point $\mathcal{P}_m$ along X_d lies in $\mathcal{F}$, there is no need for auxiliary planning. Otherwise, the agent travels to the point $n \in \mathcal{F}$ closest to $\mathcal{P}_m$.

To quantify the tracking objectives, define

$$e \triangleq x - x_\pi, \quad \hat{e} \triangleq \hat{x} - x_\pi, \quad \tilde{e} \triangleq x - \hat{x}, \tag{2}$$

where $\hat{x} : \mathbb{R}_{\geq 0} \to \mathbb{R}^D$ is the agent's open-loop state estimate, and $e, \hat{e}, \tilde{e} : \mathbb{R}_{\geq 0} \to \mathbb{R}^D$ are the *actual tracking error*,*estimated tracking error*, and *state estimation error*, respectively. The challenge is to regulate the norm of the actual tracking error to remain, eventually, below a prescribed bound.

D. Switched Controller

Let $\mathcal{S} \triangleq \{a, u\}$ be the set of indices denoting the operating modes, where a and u correspond to the modes where feedback is available and unavailable, respectively. Mode a is active when $x \in \mathcal{F}^\circ$. Mode u is active otherwise. Let $\sigma(x) \in \mathcal{S}$ denote the switching signal indicating the active subsystem. The control input takes the form $\zeta \triangleq \zeta_a(x, t)$ when $\sigma(x) = a$, and $\zeta \triangleq \zeta_u(\hat{x}, t)$ when $\sigma(x) = u$, where $\zeta_a, \zeta_u : \mathbb{R}^D \times \mathbb{R}_{\geq 0} \to \mathbb{R}^D$ are the control inputs when feedback is *available* and *unavailable*, respectively. The closed loop error system for controllers of this kind were studied in [5], Section IV.

III. Error Bounds

To facilitate the analysis, the i^{th} instant when σ switches from u to a is denoted by $t_i^a \in \mathbb{R}_{\geq 0}$ for all $i \in \mathbb{Z}_{>0}$, i.e., the instant the agent enters the interior of the feedback region. The i^{th} instant when σ switches from a to u is denoted by $t_i^u \in \mathbb{R}_{\geq 0}$, i.e., the instant the agent exits $\mathcal{F}^\circ$. Based on the switching instants, dwell-times of the i^{th} activation of the subsystems a and u are defined as $\Delta t_i^a \triangleq t_i^u - t_i^a$ and $\Delta t_i^u \triangleq t_{i+1}^a - t_i^u$, respectively.

To analyze the switched system, candidate Lyapunov-like functions are defined as

$$V_e \triangleq \tfrac{1}{2}\|e\|^2, \quad V_{\hat{e}} \triangleq \tfrac{1}{2}\|\hat{e}\|^2, \quad V_{\tilde{e}} \triangleq \tfrac{1}{2}\|\tilde{e}\|^2, \tag{3}$$

where $V_e, V_{\hat{e}}, V_{\tilde{e}} : \mathbb{R}^D \to \mathbb{R}_{\geq 0}$. To ensure a bound on the error system, the following assumption is made.

Assumption 3: Based on the design of the control input in Section II-D, it is assumed that the time derivatives of (3) yields

$$\dot{V}_e \leq -2\lambda_s V_e, \qquad \sigma = a, \tag{4}$$

$$\dot{V}_{\hat{e}} \leq -2\lambda_s V_{\hat{e}}, \qquad \sigma = u, \tag{5}$$

$$\dot{V}_{\tilde{e}} \leq \begin{cases} -2\lambda_{\tilde{e}} V_{\tilde{e}}, & \sigma = a, \\ 2\lambda_u V_{\tilde{e}} + \delta, & \sigma = u, \end{cases} \tag{6}$$

where $\lambda_s, \lambda_{\tilde{e}}, \lambda_u, \delta \in \mathbb{R}_{>0}$ are known constants.[2] ■

While the agent is in the feedback-denied region (i.e., $\sigma = u$), solving the ordinary differential inequalities in (4)–(6) and substituting in (2) and (3) yields

$$\left\|\hat{e}(t)\right\| \leq \left\|\hat{e}\left(t_i^u\right)\right\| \mathrm{e}^{-\lambda_s \Delta t}, \tag{7}$$

$$\left\|\tilde{e}(t)\right\|^2 \leq \left\|\tilde{e}\left(t_i^u\right)\right\|^2 \mathrm{e}^{2\lambda_u \Delta t} + \tfrac{\delta}{\lambda_u}\left[\mathrm{e}^{2\lambda_u \Delta t} - 1\right], \tag{8}$$

for all $t \in [t_i^u, t_{i+1}^a)$, where $\Delta t \triangleq t - t_i^u$. Since $e = \hat{e} + \tilde{e}$, and using the reset maps[3] from [5], the bounds in (7) and (8) yield

$$\|e(t)\| \leq \rho(t - t_i^u), \quad t \in [t_i^u, t_{i+1}^a), \tag{9}$$

where

$$(\rho(\Delta t))^2 \triangleq \tfrac{\delta}{\lambda_u}\left[\mathrm{e}^{2\lambda_u \Delta t} - 1\right], \tag{10}$$

and $\rho(\Delta t)$ is referred to as the *radius of uncertainty* at time t.

This bound holds for *any* trajectory under *any* controller satisfying Assumption 3, enabling the development of a dwell-time condition (Theorem 3).

IV. Criteria for Guaranteed Re-Entry

A. Preliminaries: Embedded Spheres in Euclidean Space

An embedded sphere in $\mathbb{R}^D$ is defined to be the image $C \triangleq \gamma(\mathbb{S}^{D-1})$ of an injective continuous map $\gamma : \mathbb{S}^{D-1} \to \mathbb{R}^D$. For $D = 2$, the following classical result may be applied.

Theorem 1 (Jordan-Schöenflies, see [9], Thm. E1): An injective continuous map $\gamma : \mathbb{S}^1 \to \mathbb{R}^2$ extends to a homeomorphism $\Gamma : \mathbb{R}^2 \to \mathbb{R}^2$, a continuous map with continuous inverse satisfying $\Gamma(p) = \gamma(p)$ for all $p \in \mathbb{S}^1$. The mapping Γ is called a Schöenflies extension of γ.

For higher dimensions $D > 2$, Schöenflies extensions exist under the additional condition that the embedding γ is *collared* [10], [11]. The embedding γ is collared if there is an injective continuous map $\widetilde{\gamma} : \mathbb{S}^{D-1} \times [-1, 1] \to \mathbb{R}^D$ such that $\widetilde{\gamma}(p, 0) = \gamma(p)$ for all $p \in \mathbb{S}^{D-1}$. It is well-known that polyhedral—and, more generally, piecewise-regular—maps γ (with finitely many faces) are collared (see §11 in [12]).

The interior and exterior regions of a collared embedded sphere C are defined as

$$\text{int}(C) \triangleq \Gamma\left((\mathbb{B}^\circ)^D\right), \quad \text{ext}(C) \triangleq \Gamma\left(\mathbb{R}^D \backslash \mathbb{B}^D\right), \tag{11}$$

where Γ is any Schöenflies extension of γ. It is important to note $\text{int}(C)$ and $\text{ext}(C)$ do not depend on the choice of map γ—only on its image, C. They are also independent of the choice of the Schöenflies extension Γ. Moreover, the boundary sets $\partial\text{int}(C)$ and $\partial\text{ext}(C)$ coincide with C, and C separates every point $p \in \text{int}(C)$ from every point $q \in \text{ext}(C)$ in the sense that

[2] An example of a controller satisfying the assumptions made thus far is given in Section VI of [5] where values for $\lambda_s, \lambda_{\tilde{e}}, \lambda_u$, and δ are shown to be functions of the agent dynamics and the disturbance bound $\bar{d}$.

[3] Upon each re-entry into $\mathcal{F}$, it is possible to reset the auxiliary path x_π to a new path and have $\hat{x}(t_{i+1}^a) = x(t_{i+1}^a)$ at t_{i+1}^a. In other words, the auxiliary path is updated based on the re-entry location of the agent instead of having to travel to the desired re-entry location before returning to the desired path to follow. Resetting the errors to zero results in the elimination of the minimum dwell-time condition and the vanishing of the initial conditions from the maximum dwell-time condition.

any continuous curve from p to q must intersect C. For the rest of this letter we make the following assumption.

Assumption 4: The feedback region $\mathcal{F}$ is the closure of $\mathrm{int}(C)$, where C is a collared embedded sphere in $\mathbb{R}^D$. ■

B. Construction of a "target Region"

In the notation of Section III, given t_i^u, consider a plan $\pi = (n, o, p, q)$. Alternatively, consider $\pi = (p, q)$, while setting $t_i^u = 0$. Let x_π be the associated auxiliary trajectory. Let $p = x_\pi(t_i^p)$ and $q = x_\pi(t_i^q)$, then the *initial and final uncertainty radii* for the plan π are defined as

$$\rho_{init}(\pi) \triangleq \rho(t_i^p - t_i^u)\,, \quad \rho_{fin}(\pi) \triangleq \rho(t_i^q - t_i^u)\,, \qquad (12)$$

where ρ is defined in (10). The *regions of uncertainty* are

$$U_{init}(\pi) \triangleq B_{\rho_{init}(\pi)}(p)\,, \quad U_{fin}(\pi) \triangleq B_{\rho_{fin}(\pi)}(q)\,. \qquad (13)$$

In [5] and [8], re-entry is guaranteed by selecting $q \in \mathcal{F}$ so that $U_{fin}(\pi) \subset \mathcal{F}$. This method is referred to as the *Inscribed Ball Criterion* (IBC). Treating this inclusion as a constraint results in a bound on $\rho_{fin}(\pi)$, and hence also on $\rho_{init}(\pi)$, since the function ρ is known. The example in Fig. 1 illustrates the need for a target region much larger than $\mathcal{F}$, in which to fit $U_{fin}(\pi)$, to obtain less conservative bounds. In this section such target regions are introduced.

Recall that $\mathcal{F}^\circ = \mathrm{int}(C)$. Given a point $p \in \mathrm{ext}(C)$ and a closed, connected region $R \subset \mathbb{R}^D$ with $p \in R^\circ$, define $T_{C,R}(p)$ to be the collection of all points $q \in R^\circ$ for which any smooth curve $\gamma : [0, 1] \to R^\circ$ from p to q must pass through a point of C. Let $E_{C,R}(p)$ denote the set of all $y \in C$ such that, for some $q \in T_{C,R}(p)$ there is a smooth curve $\gamma : [0, 1] \to R^\circ$ from p to q that crosses C exactly once at y.

Remark 3: In the above, one is allowed to restrict attention to smooth curves γ which intersect C transversely, i.e., their tangent line at any point of intersection with C and the tangent to C at that point together span $\mathbb{R}^D$ (see §10 of [12]).

Lemma 1: If $q \in T_{C,R}(p)$, then any curve in R from p to q must pass through a point of $E_{C,R}(p)$.

Proof: Suppose a curve $\gamma : [0, 1] \to R^\circ$ starts at point $p = \gamma(0)$ and terminates at the point $q = \gamma(1)$. Let $t' \triangleq \inf\{t \in [0, 1] : \gamma(t) \in C\}$ be the first time γ crosses C. By Remark 3, one may assume γ only crosses C transversely. Set $q' \triangleq \gamma(t')$, and let $\mathcal{U}$ be a neighborhood of q' not containing any other intersection point of γ and C such that $C \cap \mathcal{U}$ is a single interval. Find $\Delta t > 0$ such that $\gamma([t,' t' + \Delta t]) \subset \mathcal{U}$ and now set $q'' \triangleq \gamma(t' + \frac{\Delta t}{2})$. Since the curve $\gamma' \triangleq \gamma|_{[0,t'+\Delta t/2]}$ crosses C exactly once, one finds that $q'' \in \mathrm{int}(C)$ and $q' \in E_{C,R}(p)$, as required (see Fig. 3(left)).

C. Guarantee of Re-Entry Into the Feedback Region

Assume once more the agent is executing a plan $\pi = (n, o, p, q)$ over the time period $t \in [t_i^u, t_{i+1}^a]$. At time t_i^p, the agent departs in the direction of $\mathcal{F}$ by dead-reckoning to a point $q \in \mathbb{R}^D$ (note that it is possible for q to not lie in $\mathcal{F}$). For all $t \in [t_i^p, t_i^q]$, $t_i^q - t_i^p = \frac{\|q-p\|}{v_0}$ one has $x_\pi(t) = p + (t - t_i^p)v$, where $v = v_0\frac{q-p}{\|q-p\|}$. The true position $x(t)$ is guaranteed to lie in the ball $B_{\rho(\Delta t)}(x_\pi(t))$, where Δt and ρ are defined in (7) and (10), respectively.

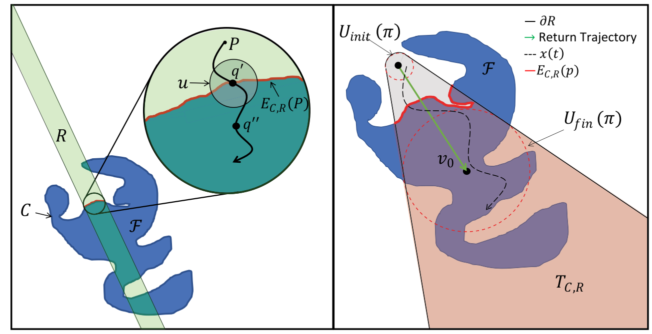

Fig. 3. Illustration of the proofs of Lemma 1 (left) and Theorem 2 (right).

Theorem 2: Suppose $U(\pi) \triangleq \bigcup_{t\in[t_i^p,t_i^q]} B_{\rho(t-t_i^u)}(x_\pi(t))$ is contained in the interior of a region R. If $U_{fin}(\pi) \subset T_{C,R}(p)$ then there exists $t \in [t_i^p, t_i^q]$ with $x(t) \in \mathcal{F}$.

Proof: If $U_{fin}(\pi) \subset T_{C,R}(p)$, then $q = x(t_i^q) \in T_{C,R}(p)$. Apply Lemma 1 to this point and the curve $\gamma : [t_i^p, t_i^q] \to R$, concluding that γ had to pass through a point of $E_{C,R}(p)$. Thus, $x(t)$ entered $\mathrm{int}(C)$ at some earlier time $t \in (t_i^p, t_i^q)$ (see Fig. 3 (right)).

Remark 4: If R is selected as a convex region, then ensuring $U_{init}(\pi) \subset R$ and $U_{fin}(\pi) \subset T_{C,R}(p)$ suffices for meeting the requirements of Theorem 2.

D. Path-Planning With Infinite Cylinders

Theorem 2 states region R should be selected so the error growth in (9) of the agent is accounted for in R up until re-entry can be guaranteed. Since an upper bound on the error growth rate is given in (9), R may be designed to contain all possible trajectories of $x(t)$, given a plan $\pi = (n, o, p, q)$. In principle, given the reference point of departure $p = x_\pi(t_i^p)$ and a reference target velocity vector v with $\|v\| = v_0$, R could always be selected to be the (unbounded) *cone of uncertainty* $\bigcup_{t\in[t_i^p,\infty)} B_{\rho(t-t_i^u)}(p + (t - t_i^p)v)$ in that direction. However, this choice is challenging from a computational perspective, because of the non-linearity of ρ.

Given any point $p \in \mathcal{F}^c$, the planner needs to select q and a region R best suited for guaranteeing the agent's return to $\mathcal{F}$. In general, to apply Theorem 2 a rich collection $\mathcal{R}(p)$ of regions R satisfying $p \in R^\circ$ with "sufficiently large" $T_{C,R}(p)$ for some $R \in \mathcal{R}(p)$ must be designed.

Fig. 4 presents two alternatives to the approach using cones of uncertainty: the cylindrical geometry in Fig. 4(A) and a conical geometry in Fig. 4(B). The subsequent development only considers the cylindrical geometry, in the interest of reducing computational cost. Specifically, consider

$$\mathcal{R}(p) \triangleq \left\{R_{p,v,w} : v \in \mathbb{R}^D, \|v\| = v_0, w > 0\right\}, \qquad (14)$$

where $R_{p,v,w}$ is the solid cylinder of radius w whose axis passes through p and has direction v (see Fig. 4(A)),

$$R_{p,v,w} \triangleq \left\{z \in \mathbb{R}^D : \left\|(z - p) - \frac{(z-p)\cdot v}{v_0^2}v\right\| \leq w\right\}. \quad (15)$$

A pair (v, w) will be referred to as *return parameters*. For $R = R_{p,v,w}$, the following observations are made.

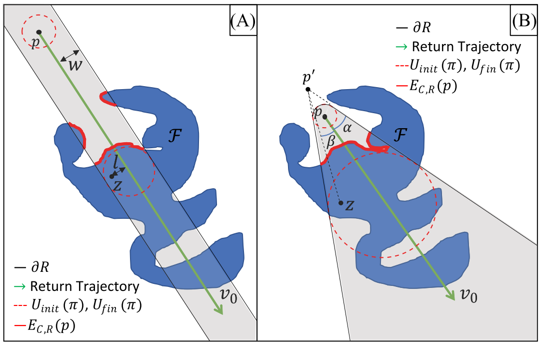

Fig. 4. Illustrations of possible target regions R for use with the planner. The "cylinder" geometry implemented in this letter is shown in A. More general geometries are possible (for example the "conical" region shown in B), but are not discussed here due to higher computational overhead.

- For excessively large values of w (e.g., w big enough for $C \subset R$) one has $T_{C,R}(p) = \mathcal{F}$. Therefore, any ball contained in $T_{C,R}(p)$ provides little improvement upon IBC of guaranteeing return.
- More generally, note that $R \setminus C$ has no more than two unbounded components. When there is only one such component, the existence of a ball of radius w contained in $T_{C,R}(p)$ cannot be guaranteed.
- In all other cases, the collection of balls of radius w contained in $T_{C,R}(p)$ is non-empty: a point of the form $q = p + \alpha v$ always exists with $\alpha > 0$ and $B_w(q) \subset T_{C,R}(p)$ (see Fig. 4(A)).

The developed planner seeks to maximize the arc length from o to p along X_d subject to the constraint of re-entry being guaranteed by $\mathcal{R}(p)$. As a result, maximizing $t_i^p - t_i^u$ subject to the existence of a point $q = p + \alpha v$ with $B_w(q) \subset T_{C,R}(p)$ and $R = R_{p,v,w}$ provides a *lower bound* on the time the agent could spend tracking X_d, which the planner seeks to maximize.

$$\Delta t^* \triangleq \max_{p,v,w,\alpha} \left(\rho^{-1}(w) - \alpha\right)$$
$$\text{s.t.} \begin{cases} B_w(p + \alpha v) \subset T_{C,R}(p), \\ R = R_{p,v,w} \in \mathcal{R}(p), \end{cases} \tag{16}$$

given a ball $B_w(q) \subset T_{C,R}(p)$. To guarantee re-entry, it is required that $x(t_i^q) \in B_w(q)$ and $\rho(t_i^q - t_i^u) \leq w$. It then follows that $t_i^p - t_i^u \leq \rho^{-1}(w) - \alpha$ because $\alpha = t_i^q - t_i^p$.

For each $R = R_{p,v,w} \in \mathcal{R}(p)$, the *Maximum Allowed Uncertainty Radius (MAUR)* is defined as

$$\mathtt{MAUR}(p, v, w) \triangleq \max_{\alpha > 0} \rho(\rho^{-1}(w) - \alpha)$$
$$\text{s.t. } B_w(p + \alpha v) \subset T_{C,R}(p), \tag{17}$$

representing the agent's budget of uncertainty at the point p for the return parameters v, w.

In practice, assuming the distance between any two consecutive way points along X_d does not exceed some small $\epsilon > 0$, the optimization in (16) ranges over all $p = \mathcal{P}_{m'}$, $m' \geq m$, where m satisfies $o = \mathcal{P}_m$. Note that it is possible for the optimal p to satisfy $p = o$. Hence, an optimal path plan, $\pi^* = (n^*, o, p^*, q^*)$, will be given by

$$n^* \triangleq \arg\min_n \{\mathtt{dist}(n, o) : n \in \mathcal{F}\}, \tag{18}$$

$$(p^*, v^*, w^*, \alpha^*) \triangleq \arg\max_{p,v,w,\alpha} \left(\rho^{-1}(w) - \alpha\right), \tag{19}$$

$$q^* \triangleq p^* + \alpha^* v^*, \tag{20}$$

subject to the same constraints as (16), and noting that $p = x_{\pi^*}(\Delta t^*)$ is an implicit constraint on π^*.

E. Dwell-Time Analysis

Definition 2 (Feasible Region): For every point $p \in \mathcal{F}^c$, let the *feasible region* $\mathcal{G}$ be defined by

$$\mathcal{G} \triangleq \mathcal{F} \cup \{p \in \mathcal{F}^c : v_0^{-1}\mathtt{dist}(p, \mathcal{F}) < \tau(p)\}, \tag{21}$$

where $\tau(p) \triangleq \max_{v,w,\alpha}\{\rho^{-1}(w) - \alpha\}$, subject to $B_w(p + \alpha v) \subset T_{C,R}(p)$ and $R = R_{p,v,w}$. The *feasible region for initialization* is defined by

$$\mathcal{G}_0 \triangleq \mathcal{F} \cup \{p \in \mathcal{F}^c : \tau(p) > 0\}. \tag{22}$$

Theorem 3: Suppose an agent is given whose motion is governed by (1) and the controller from Section II-D. Moreover, suppose Assumptions 1–3 are satisfied. Let $\mathcal{F}$ be a region satisfying Assumption 4. Also suppose that, given $x(0) \in \mathcal{G}_0$ and $e(0) = \hat{e}(0) = \tilde{e}(0) = 0$, the agent executes a sequence of plans as follows: (a) if $x(0) \in \mathcal{F}$ then let $\pi_i = (n_i, o_i, p_i, q_i), i \geq 1$ each with an associated region $R_i \in \mathcal{R}(p_i)$ as defined in (14); (b) otherwise, let $\pi_0 = (p_0, q_0)$ with $p_0 = x(0)$ and an associated region $R_0 \in \mathcal{R}(p_0)$, followed by a sequence of plans as in (a). If, between plan executions the agent is confined to $\mathcal{F}$, and all the plans satisfy the re-entry condition of Theorem 2—that is $U_{fin}(\pi_i) \subset T_{C,R_i}(p_i)$ for all i—then the actual tracking error is ultimately bounded, uniformly over $\mathcal{G}_0$ and the set of plans, provided the switching signal satisfies the maximum dwell-time condition $\rho(\Delta t_i^u) \leq \rho_{fin}(\pi_i)$, written explicitly as

$$\Delta t_i^u \leq \frac{1}{2\lambda_u} \ln\left(\frac{\lambda_u\left(\rho_{fin}(\pi_i)\right)^2}{\delta} + 1\right), \tag{23}$$

where $\rho_{fin}(\pi_i)$ is defined in (12).

Proof: For $x(0) \in \mathcal{G}_0 \setminus \mathcal{F}$ it takes at most $\rho^{-1}(\mathtt{diam}(\mathcal{F}))$ time to acquire feedback. Therefore, without loss of generality assume $x(0) \in \mathcal{F}$. With Assumptions 1–3 satisfied, suppose that plan π_i also satisfies $U_{fin}(\pi_i) \subset T_{C,R_i}(p_i)$. By Theorem 2, x is guaranteed to re-enter into the feedback region $\mathcal{F}$, while $\rho_{fin}(\pi_i)$ bounds the error growth from above. One can then apply the proof of Theorem 1 in [5] to deduce that the tracking error is ultimately bounded uniformly over $\mathcal{G}_0$ and the set of plans, since it satisfies the dwell-time condition (23).

Theorem 4: Suppose X_d is a polygonal curve contained in the feasible region $\mathcal{G}$. Then X_d can be tracked with a guarantee of re-entry, for any initial condition $x(0) \in \mathcal{G}_0$, provided the error system is initialized with $e(0) = \hat{e}(0) = \tilde{e}(0) = 0$.

Proof: Suppose X_d is a polygonal curve contained in the feasible region $\mathcal{G}$. For each m, let $\nu(m)$ denote the smallest $m' > m$ such that $\mathcal{P}_{m'} \notin \mathcal{F}$. The proof proceeds by induction. For the base step, at time $t = 0$, if $x(0) \in \mathcal{F}$ then set $t_1^a = 0$;

otherwise, the agent executes $\pi_0 = (p_0, q_0)$ with $p_0 = x(0)$ and $q_0 = x(0) + \alpha_0 v_0$, where (v_0, w_0, α_0) realizes the maximum in the definition of $\tau(x(0))$. By Theorem 2, entry into $\mathcal{F}$ is guaranteed, resulting in $t_1^a \in [0, \alpha_0]$. For the induction hypothesis, assume plans $\pi_i = (n_i, o_i, p_i, q_i = p_i + \alpha_i v_i), i = 1, \ldots, k$ have been constructed so that (a) $o_1 = \mathcal{P}_0$; (b) $p_i = \mathcal{P}_{m_i}$ with $1 < m_1 < \cdots < m_k$; (c) $o_{i+1} = \mathcal{P}_{\nu(m_i)}$ for $i = 1, \ldots, k-1$; and (d) the conditions of Theorem 3 hold.

Let $x : [0, t_{k+1}^a] \to \mathbb{R}^D$ be an execution of these plans and note $x(t_{k+1}^a) \in \mathcal{F}$. For the induction step, compute a point $n_{k+1} \in \mathcal{F}$ at minimum distance to $o_{k+1} \triangleq \mathcal{P}_{\nu(m_k)}$. Select π_{k+1} to be the optimal plan $\pi^* = (n^*, o, p^*, q^* = p^* + \alpha^* v^*)$ from Section IV-D, for a choice of $n^* = n_{k+1}$ and $o = o_{k+1}$. Set $p_{k+1} = p^*$, $\alpha_{k+1} = \alpha^*$, $v_{k+1} = v^*$, and $q_{k+1} = q^*$.

Now extend x as follows: first, the agent proceeds from $x(t_{k+1}^a)$ to n_{k+1} through $\mathcal{F}$—while tracking X_d, if $\nu(m_k) > m_k + 1$—defining the behavior of x over the time interval $[t_{k+1}^a, t_{k+1}^u]$; next, the agent executes the plan π_{k+1}, which guarantees re-entry into $\mathcal{F}$ at some time $t_{k+2}^a \le t_{k+2}^q$. Now it is required to show that the dwell-time condition $\rho(\Delta t_{k+1}^u) \le \rho_{fin}(\pi_{k+1})$ of Theorem 3 is satisfied.

Since ρ is strictly increasing, this is equivalent to requiring $\Delta t_{k+1}^u \le \rho^{-1}(\rho_{fin}(\pi_{k+1})) = t_{k+1}^q - t_{k+1}^u$. Recalling that $\Delta t_{k+1}^u = t_{k+2}^a - t_{k+1}^u$ finishes the argument.

Remark 5: Note the path plan π_{k+1} in the proof covers the range of consecutive way points $o_{k+1} = \mathcal{P}_{\nu(m_k)}, \ldots, \mathcal{P}_{m_{k+1}} = p_{k+1}$ along X_d, $\nu(m_k) \ge m_k + 1$, while the preceding plan π_k covered the range $o_k = \mathcal{P}_{\nu(m_{k-1})}, \ldots, \mathcal{P}_{m_k} = p_k \subset X_d$. Hence, progress will be made along X_d by any execution of π_{k+1}. In particular, there are no Zeno executions.

V. Precomputation and Plan Generation

Since the geometry of the feedback region and the evolution of the region of uncertainty are known, a brute-force algorithm can be used to obtain all of the needed information for future path-planning, provided the way points $\mathcal{P}_m$, $m = 0, \ldots, M-1$, form a subdivision of X_d of sufficiently fine mesh[4] $\epsilon > 0$. For each m, an approximation to the solution of the optimization problem (16) for $\mathcal{P}_m$ is obtained by solving for $\mathtt{MAUR}(\mathcal{P}_m, v, w)$—see (17)—over a sufficiently dense range of possible return parameters (v, w), and storing the solution in a data-set. The plans π_i constructed in the preceding section are then selected based on the information in the *data-set* to satisfy the mission objectives. To select a return trajectory, the agent solves the optimization problem in (19) by executing a search over the data-set.

To construct the data-set, for each $\mathcal{P}_m$, $m = 0, \ldots, M-1$, return parameters (v_j, w_k), $v_j \triangleq v_0[\cos(\theta_j), \sin(\theta_j)]$ are used, $\Theta \triangleq \{\theta_j \triangleq 2\pi j/J : j = 0, \ldots, J-1\}$, and $W \triangleq \{w_0, \ldots, w_{K-1}\} \subset \mathbb{R}_{\ge 0}$. Given the feedback region $\mathcal{F}$, Algorithm 1 computes $T_{C,R}(\mathcal{P}_m)$ for each $R = R_{\mathcal{P}_m, v_j, w_k}$. Next, the nearest return target and associated MAUR are computed:

$$q_{m,j,k} \triangleq \mathcal{P}_m + \alpha_{m,j,k} v_j, \tag{24}$$

[4]Recall that a subdivision S of X_d has mesh $\mu(S) \le \epsilon$ if $\mathtt{dist}(p, q) \le \epsilon$ for every pair of consecutive points p, q in the subdivision.

Algorithm 1: Data-Set for R.

Require: X_d as a list of points $\mathcal{P}_0, \ldots, \mathcal{P}_{M-1} \in \mathbb{R}^D$
Require: $\mathcal{F} = \mathtt{cl}(\mathrm{int}(C))$, C given as a sequence of vertices
for $m := 0$ to $M-1$ **do**
  $p \leftarrow \mathcal{P}_m$
  for $j := 0$ to $J-1$ **do**
    $v \leftarrow v_0 \cdot [\cos\frac{2\pi j}{J}, \sin\frac{2\pi j}{J}]$
    for $k := 0$ to $K-1$ **do**
      $w \leftarrow w_k$
      $R \leftarrow R_{p,v,w}$
      $T_{C,R}(p) \leftarrow$ FindTargetRegionp, R, v, w
      $q_{m,j,k} \leftarrow$ FindTargetPoint$p, v, w, T_{C,R}(p)$
      $\rho_{m,j,k} \leftarrow$Equation (26)
return $(q_{m,j,k}, \rho_{m,j,k})_{m=0,j=0,k=0}^{M-1,J-1,K-1}$
functionFindTargetRegion(p, R, v, w)
  $A \leftarrow R \setminus \mathcal{F}$
  for all $a \in$ regions$A$ **do**
    if $p \in \mathring{a}$ **then**
      $B \leftarrow a$
      Exit
  return $R \setminus B$
function FindTargetPoint(p, v, w, t)
  $\alpha^* \leftarrow \min\{\alpha > 0 : B_w(p + \alpha v) \subseteq T\}$
  return $p + \alpha^* v$
function Regions$A$
  return the list of connected components of A

$$\alpha_{m,j,k} \triangleq \min\left\{\alpha > 0 : B_{w_k}(q_{m,j,k}) \subset T_{C,R}(\mathcal{P}_m)\right\}, \tag{25}$$

$$\rho_{m,j,k} \triangleq \rho\left(\rho^{-1}(w_k) - \alpha_{m,j,k}\right). \tag{26}$$

Note that $\rho^{-1}(w_k) - \alpha_{m,j,k} \le 0$ means $\mathcal{P}_m \notin \mathcal{G}$, in which case X_d cannot be tracked with a guarantee of re-entry using this method. Also note that $v_0 \alpha_{m,j,k} = \mathtt{dist}(\mathcal{P}_m, q_{m,j,k})$.

Upon termination, the result is a three dimensional array denoted by $\rho_{m,j,k} \in \mathbb{R}^{M \times J \times K}$, where each element of the array is the MAUR at point $\mathcal{P}_m \in X_d$, associated with a return trajectory $\theta_j \in \Theta$, and a width $w_k \in W$.

Remark 6: In some applications, it may be necessary to further restrict the MAUR to ensure a certain degree of accuracy while tracking X_d. If this is the case, the user may use this predetermined desired upper bound as long as it is less than the MAUR at the point of departure.

A. Algorithm Simplification (Algorithm 2)

The size of the data-set, $M \times J \times K$, can easily become prohibitive for optimization by brute force search. To reduce the search space, some of the iterations for the different $R \in \mathcal{R}(\mathcal{P}_m)$ may be bypassed by selecting a single return trajectory and/or single width. In the numerical experiments in Section VI, a single pair of return parameters, (v, w) is assigned to each $\mathcal{P}_m$. Specifically, v is set to equal the vector which bisects the smallest sector emanating from $\mathcal{P}_m$ and containing $\mathcal{F}$; next, w is selected as the largest $w_k \in W$ such that $R = R_{\mathcal{P}_m, v, w_k}$ satisfies $T_{C,R}(p) \ne \mathcal{F}$. This results in the data-set having size

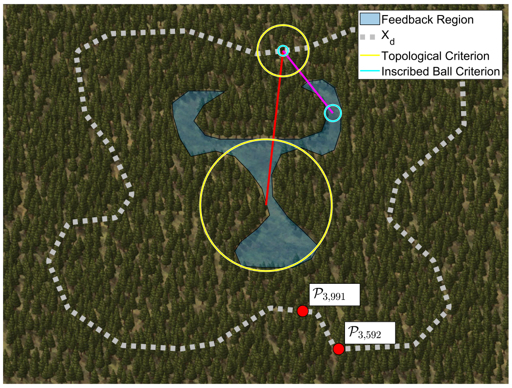

Fig. 5. Comparison of criteria for guaranteed re-entry at a point. The MAUR for the topological criterion is larger than that of IBC. Hence, the agent can afford more uncertainty about its position while guaranteeing re-entry along a different path (red instead of magenta). Note the IBC return trajectory (magenta) is shorter, indicating a possible trade-off between maintaining tracking uncertainty budgets and minimizing deviation from the desired path—a topic for future study.

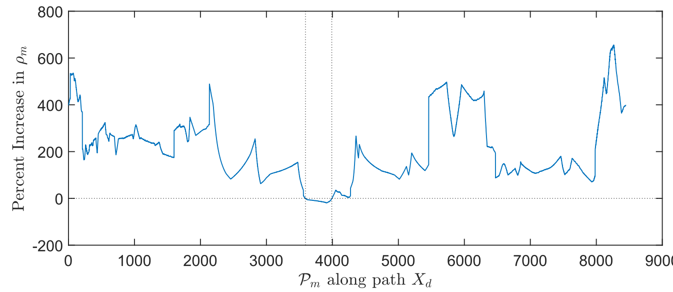

Fig. 6. Percent increase, μ_m, in the MAUR at the point of departure $\mathcal{P}_m \in X_d$ using the proposed criterion for guaranteed re-entry. Note $\mu_m < 0$ between $\mathcal{P}_{3592}$ and $\mathcal{P}_{3991}$ (vertical dashed lines).

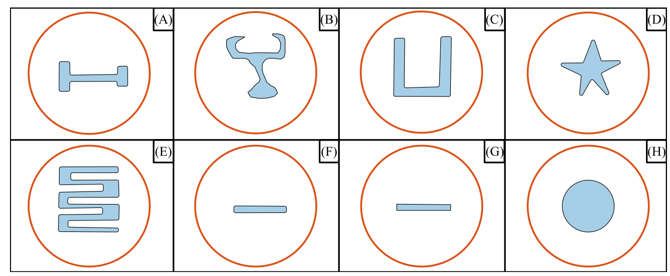

Fig. 7. Geometries: (A) Dumbbell, (B) Generic, (C) Horseshoe, (D) Star, (E) Switchback, (F) Rounded Rectangle, (G) Standard Rectangle, (H) Circle.

M. Algorithm 2 assigns the largest possible radius of uncertainty ρ_m to the points q_m, but it may fail to account for the effects of the distance traveled from $\mathcal{P}_m$ to q_m. In (26), maximizing w_k may come at the expense of α_m having to become large, as well. Ultimately, this simplification trades geometric information for computational efficiency.

VI. Numerical Experiments

Experiments were conducted in MATLAB to investigate different geometries for the feedback region. In each experiment the MAURs ρ_m generated by the Algorithm 2 (Section V-A) are compared[5] with the corresponding MAURs—denoted by ρ'_m—generated by IBC.

Experiment, A Generic Example. The task space is a rectangular region in the plane with unitless dimensions $2{,}048 \times 1{,}536$. Generic polygonal feedback region $\mathcal{F}$ and desired path X_d were hand-drawn (see Fig. 5). X_d was then subdivided to ensure a mesh size at most 1, resulting in 8,449 way points. The parameters are $\lambda_u = 3$, $\delta = 5$, and $v_0 = 2{,}000$, to ensure $\rho'_m > 0$ exists for all m.

Fig. 6 plots the percent increase $\mu_m \triangleq \frac{\rho_m - \rho'_m}{\rho'_m} * 100$ as a function of m. The plot indicates that Algorithm 2 provides a significant improvement over IBC for this specific geometry. However, IBC outperforms Algorithm 2 ($\mu_m < 0$) for points $\mathcal{P}_{3{,}592}$ to $\mathcal{P}_{3{,}991}$ (see Fig. 6; also see the points marked in Fig. 5). This reduction in the performance of Algorithm 2 results from the MAUR being generated from only one pair of return parameters. Had Algorithm 1 been deployed instead of Algorithm 2, the list of possible return trajectories would have included the one suggested by IBC, guaranteeing $\mu_m \geq 0$ at every point. Despite its sub-optimal performance, for this geometry, Algorithm 2 provides an average improvement of 209% over IBC, with the largest value of μ_m being 656%.

[5]The typical run time for Algorithm 2 in the experiments presented is about an hour. Consequently, running Algorithm 1 on all the experiments would require weeks of computation time, motivating Algorithm 2.

Experiment: Sample Geometries. To gain more insight into the interaction between the uncertainty radii and the geometry of the feedback region, a select number of example feedback regions was considered (see Fig. 7). In geometries A–G, the polygons were hand drawn, and the circular region H was approximated by a regular polygon with 100 vertices.

The same parameters were used in these experiments that were used in Section VI. A polygonal approximation of a circle is used as the desired path X_d. To ensure the same mesh requirement, 6,401 vertices was used. The initial point $\mathcal{P}_1$ along X_d is the rightmost point of the circle, with X_d oriented counter-clockwise.

Baseline Experiment, Concentric Circles. As a baseline for comparing the two methods, we replicate the settings of [5]. C and X_d were taken to be (approximate) concentric circles (see Fig. 7(H)). The two methods render near identical results: the value of μ_m fluctuates at high frequency between -0.21% and 2.74%. The fluctuations are caused by the discrete approximation of the circular boundary of the feedback region C by a regular polygon.

Baseline Experiment, Rectangles. Fig. 8 plots the functions μ_m for the two rectangular geometries (see Fig. 7(F,G)) and confirms the intuitive argument, presented in the introduction (Fig. 1), behind Algorithms 1 and 2.

Also, note how the sharp corners of the standard rectangle cause ρ'_m to approach zero, resulting in the spikes in μ_m visible in the figure. This spiking is due to the fact that, for points $\mathcal{P}_m$ whose nearest point projection to $\mathcal{F}$ results in a return trajectory collinear with an edge of the rectangle, no inscribed ball can be constructed. Fig. 8 demonstrates how rounding the corners mitigates this problem.

Comparing Multiple Geometries. Fig. 9 presents a comparison of the functions μ_m for the geometries in Fig. 7(A–F).

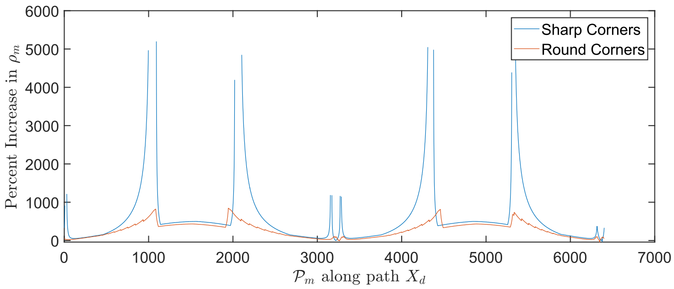

Fig. 8. Percent increase, μ_m, in the MAUR for two types of rectangular feedback regions. One with sharp corners and one with rounded corners.

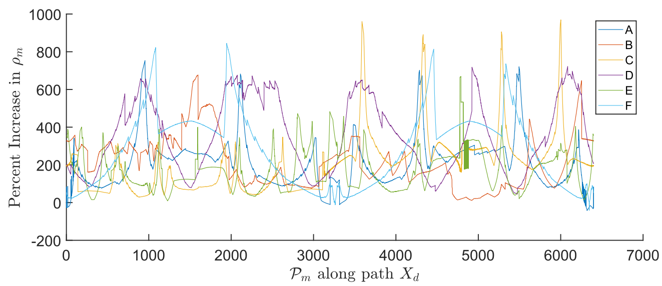

Fig. 9. Percent increase, μ_m, in the MAUR at the point of departure from X_d for a variety of geometries.

The observation made in Section VI, motivated "rounding" the corners of all the feedback region shapes.

Given these experiments (see Fig. 9), with a total of $46{,}855$ data points (including the generic example), the mean-average increase in the maximum allowed radius of uncertainty was found to be 233%. The largest mean-average for a single geometry was 354%. This was observed in the "star" geometry (see Fig. $7(D)$). The smallest mean-average for a single geometry was 168%. This was observed in the "switchback" geometry (see Fig. $7(E)$). The largest increase at a single point was found to be 969%. This was observed in the "horseshoe" geometry (see Fig. $7(C)$). The smallest was found to be -42%. This was observed in the "dumbbell" geometry (see Fig. $7(A)$).

Overall, it was shown that, even across a range of unique geometries, the topological criterion for guaranteed re-entry in Theorem 2 is superior to IBC, in terms of MAUR. The topological criterion was shown to render large improvements even though the sub-optimal Algorithm 2 was used instead of Algorithm 1. It is expected that Algorithm 1, with a much richer data-set, would generate larger values for the optimal MAUR. Moreover, Algorithm 1 is guaranteed to remove any instances where IBC outperforms the topological method. This guarantee is due to the fact the richer data-set would include the suggested return trajectories generated by IBC.

VII. Conclusion

Given an autonomous agent in Euclidean space, a topologically motivated method for guaranteeing re-entry of the agent into a feedback region was developed, with the aim of extending the reach of existing methods to include arbitrary geometries of the feedback region. This method was integrated into an existing framework for developing dwell-times for an autonomous system tasked with following a desired path in the presence of intermittent state feedback. A path-planning algorithm leveraging the new topological re-entry criterion is presented and evaluated against the same planner using IBC for synthetic and generic example geometries. The new topological method was shown to increase the time an agent is able to safely operate in a feedback-denied region, for a variety of geometries. A simplified and sub-optimal implementation of the new method yields improvements in the allowed error growth by hundreds of percentage points. This outcome, as well as computational inefficiencies in the current algorithm, motivate future investigation along several lines of inquiry. Among these, more efficient methods for computing MAURs and optimizing the choice of return trajectories, as well as a method for implementing the "cone of uncertainty"—rather than an infinite strip—as a target region (Section IV-D), are of great interest to the future development of an optimal implementation. Future research will also focus on applying the topological criterion for guaranteed re-entry to the task of optimizing traditional long-term tracking objectives such as total time to task completion, rather than merely maximizing each individual segment.

Acknowledgment

Any opinions, findings, and conclusions or recommendations expressed in this material are of the author(s), and do not necessarily reflect the views of the sponsoring agency.

References

[1] G. Palmieri, M. Palpacelli, M. Battistelli, and M. Callegari, "A comparison between position-based and image-based dynamic visual servoings in the control of a translating parallel manipulator," *J. Robot.*, vol. 2012, 2012, Art. no. 103954.

[2] A. J. Davison, I. D. Reid, N. D. Molton, and O. Stasse, "Monoslam: Real-time single camera slam," *IEEE Trans. Pattern Anal. Mach. Intell.*, vol. 29, no. 6, pp. 1052–1067, Jun. 2007.

[3] N. E. Leonard and A. Olshevsky, "Cooperative learning in multi-agent systems from intermittent measurements," in *Proc. IEEE Conf. Decis. Control*, Florence, Italy, Dec. 2013, pp. 7492–7497.

[4] E. Garcia and P. J. Antsaklis, "Model-based event-triggered control for systems with quantization and time-varying network delays," *IEEE Trans. Autom. Control*, vol. 58, no. 2, pp. 422–434, Feb. 2013.

[5] H.-Y. Chen, Z. I. Bell, P. Deptula, and W. E. Dixon, "A switched systems framework for path following with intermittent state feedback," *IEEE Control Syst. Lett.*, vol. 2, no. 4, pp. 749–754, Oct. 2018.

[6] F. Zegers, H.-Y. Chen, P. Deptula, and W. E. Dixon, "Distributed Coordination of Multiple Unknown Euler-Lagrange Systems," in *Proc. IEEE Trans. Cont. Network Syst.*, vol. 5, no. 1, 2018, pp. 55–66.

[7] D. Liberzon, *Switching in Systems and Control*. Cambridge, MA, USA: Birkhauser, 2003.

[8] D. Le, H.-Y. Chen, A. R. Teel, and W. E. Dixon, "Path following with stable and unstable modes subject to time-varying dwell-time conditions," *IFAC World Congr.*, Berlin, Germany, July, 2020.

[9] J. Gallier and D. Xu, *A Guide to the Classification Theorem for Compact Surfaces*. Berlin, Germany: Springer, ch. Appendix E., pp. 157–163, 2012.

[10] A. Hatcher, Algebraic Topology. Cambridge Univ. Press, Cambridge, 2002, [Online]. Available: http://www. math. cornell.edu/ hatcher/AT/ ATpage. html

[11] M. Brown, "A proof of the generalized schoenflies theorem," *Bull. Amer. Math. Soc.*, vol. 66, no. 2, pp. 74–76, 1960.

[12] R. Burns, B. Dubrovin, A. Fomenko, and S. Novikov, *Modern Geometry-Methods and Applications: Part II: The Geometry and Topology of Manifolds*. Berlin, Germany: Springer, 2012.